V International Conference on Particle-based Methods – Fundamentals and Applications
PARTICLES 2017
P. Wriggers, M. Bischoff, E. Oñate, D.R.J. Owen, & T. Zohdi (Eds)

COUPLED DISTINCT ELEMENT METHOD COMPUTATIONAL FLUID DYNAMICS ANALYSES FOR RESERVOIR LANDSLIDE MODELLING

S. UTILI[1], T. ZHAO[2], GB CROSTA[3],

[1] School of Civil Engineering and Geosciences, Newcastle University,
Drummond Building, Newcastle upon Tyne, United Kingdom
stefano.utili@newcastle.ac.uk

[2]College of Water Resource and Hydropower, Sichuan University,
Chengdu, China
tzhaoslide@outlook.com

[3] Department of Earth and Environmental Sciences, Universita degli studi Milano Bicocca,
Piazza della Scienza 4, 20126 Milano, Italy
giovannibattista.crosta@unimib.it

Key words: Vajont landslide, impulse wave, rapid rockslide, coupled DEM-CFD.

Abstract. The Vajont landslide involved a large mass of rock splashing at high speed into the reservoir which in turn generated a high impulse water that overtopped the dam and swept away the downstream village. In several cases of reservoir landslide, albeit the flood defence structures may remain intact, a catastrophe still occur due to the generation of a ‚tsunami' wave. Since the features of the tsunami wave strongly depend on the physics of the rock splashing and the subsequent rock – water interaction, a numerical tool accounting for such physics is required for predictions to be reliable.

Here, the formulation of a coupled 3D Distinct Element Method (DEM) – Computational Fluid Dynamics (CFD) code used to simulate the rock slide from onset to impact with the reservoir and the subsequent generation of the impulse wave, is presented. To run realistic simulations in an affordable runtime, coarse graining is employed. The main results of quasi 3D analyses in plane strain along two cross-sections representative of the eastern and western slope sectors are presented. The results show to be in broad agreement with the available recorded observations.

1 INTRODUCTION

Landslide generated waves can be major hazards for developed areas on reservoirs, fjords, and lakes because the large mass and kinetic energy of landslides can generate waves that release tremendous forces on surrounding coastal areas and hillslopes. Damage caused by landslide tsunami runup can extend to areas well-above the shoreline, endanger human life, and cause major economic impacts, as indicated by large events that have occurred in recent history. A recent example is the 3 million m3 rockslide impacted Chehalis Lake in British Columbia, Canada, in 2007, generating a wave that stripped vegetation to elevations over 38 m above the shoreline [1,2]. The tsunami left a deposit of woody debris that formed a dam at the lake outlet,

exposing a downstream community to outburst flood hazards and requiring a lengthy and costly debris removal program [2]. [3] have presented a new set of experiments run in the laboratory at reduced scale that together with the theoretical study of [4] provide a first theoretical conceptual framework to study tsunamis generated by granular landslides. From their valuable dimensional analysis, it emerges that several physical parameters affect the generation of the tsunami and behaviours ranging from a wave whose amplitude quickly attenuates completely to a wave that propagates unabated are possible.

Among all the landslide induced tsunamis the most investigated event is indeed the Vajont rockslide [5] which is the object of this paper. The landslide involved approximately 270 million m^3 of rock and generated water waves probably averaging 90 m above the dam crest. 100 and 200 metres high water wave traces were observed along the left and right valley flanks, respectively [6]. The displaced water initially raised along the opposite valley flank and then overtopped the dam flooding successively the downstream village of Longarone, along the Piave river valley, causing more than 2,000 casualties.

Even though parallel computation techniques have been developed, the number of particles which can be simulated on PCs or PC clusters is still far smaller than that typical of real slopes (*e.g.* thousands of billions of grains). To overcome this problem, coarse graining (Sakai et al. 2012) is employed. In this technique, a coarse particle represents a collection of real fine particles. As a result, a large-scale DEM simulation of granular flow can be performed using a relatively small number of calculated particles [7].

The theory and methodology of the DEM-CFD coupling model are introduced in the next section together with the governing equations for particle motion, particle-fluid interaction and fluid flow. In the following section, the coarse graining technique is described. Finally, the main results of the simulations of the Vajont event are summarised.

2 THEORY AND METHODOLOGY

The DEM code ESyS-Particle [8] and the CFD code OpenFOAM [9] were employed for the simulations presented here. The coupling algorithm originally written in YADE [10] was implemented in ESyS-Particle by the authors [11]. The mechanical contact law between solid particles is based on linear springs and frictional tangential sliders plus rolling resistance [12].

The fluid–particle interaction force consists of two parts: hydrostatic and hydrodynamic forces. The hydrostatic force acting on a single particle, *i*, accounts for the influence of fluid pressure gradient around the particle, i.e. buoyancy [13]. The hydrodynamic forces acting on a particle are the drag, lift and virtual mass forces; the latter two forces being neglected. The drag force acting on an individual solid particle is here calculated using the empirical correlation proposed by [14]. The drag force coefficient is defined according to the correlation proposed by [15].

The governing equations of fluid flow in a fluid–solid mixture system can be derived from the theory of multi-phase flow [16], in which the free surface condition is resolved by the Volume of Fluid method [17]. In our numerical simulations, the fluid domain is initially discretized into a series of mesh cells, in which the solid particles may be dispersed. In each fluid mesh cell, the volume fraction of the summation of fluid phases is n (i.e. porosity), for

which, the volume fraction occupied by the fluid phase 1 (e.g. water) is β ($0 \leq \beta \leq 1$), while it is 1 - β for the other phase.

3 COARSE GRAINING TECHNIQUE

We assume that: (1) one large particle represents a clump of real sized sand grains (see Fig. 1); (2) the fine grains are bonded together, so that they can move as a whole; (3) the translational and rotational motion of the coarse grain and the clump of fines grains are the same; (4) the contact forces acting on the coarse grains are the summation of contact forces acting on this clump of real grains by the neighbouring grains. The fluid viscous drag force acting on the coarse particle is calculated by balancing the coarse particle and a clump of real particles. This particle scale up method is called e ‘‘coarse grain model’’ in the literature [7].

Denoting the sizes of the coarse grain particle and original real sand particle as D and d respectively, the number of particles (N) in the clump can be approximated as: $N = D^3/d^3$. The drag force acting on the clump is the summation of the drag forces acting on all the grains. Thus, the drag force on a scaled particle in the CFD-DEM code should be scaled up by a factor α with $\alpha = F_d/F'_d$, F_d the drag force acting on the clump and the drag force acting on the scaled particle. By setting the Reynolds numbers the same, the values of the drag force coefficient are the same for both the real fluid flow and the numerical models, so $\alpha = D/d$. Simulations were run for different values of α. As shown in Table 1, α was set to 1, 5 and 10, so that one large particle in the DEM can represent a clump of fine grains ranging in number from 1 to 10^3. The hydrostatic forces acting on a coarse particle and a clump of fine grains are the same, because it is determined only by the volume of solid materials. It is also noted that other parameters for the coarse and real particles are the same, so that realistic soil properties can be modelled in numerical simulations.

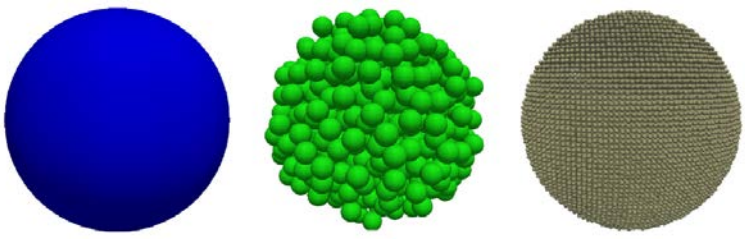

Fig. 1 Schematic view of the scaling law used in the DEM, α is the scaling factor.

4 RESULTS OF THE NUMERICAL SIMULATIONS

A plan view of the Vajont rockslide is shown in Fig. 2a, together with the traces of the two cross sections A–A and B–B, representative of the eastern and western sectors of the slide, and herein analysed. The profiles along these cross sections are illustrated in Fig. 2b and 2c. Details of the generation procedure of the slope mass are given in [18].

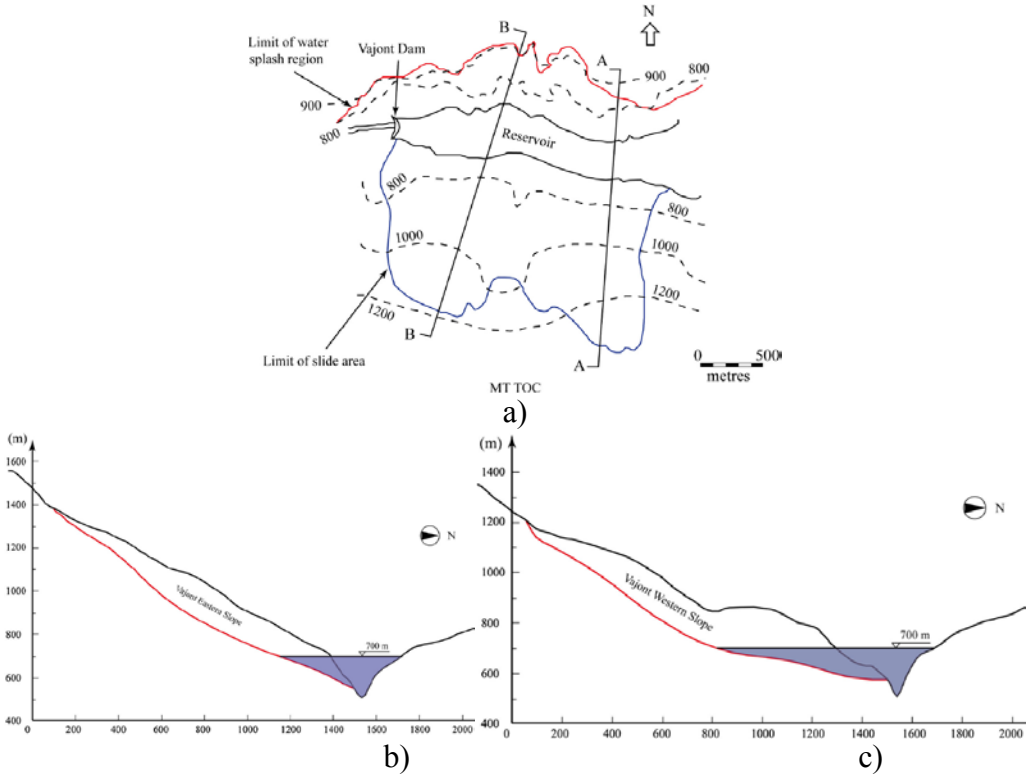

Fig. 2 a) Plan view of the Vajont rockslide with the straight lines indicating the cross sections A-A and B-B corresponding to the easter and western slopes of the Vajont valley respectively; b) profile of the eastern slope; c) profile of the western slope. The water reservoir is in blue.

The input parameters adopted for both the DEM and CFD models are listed in Table 1 and have been chosen ac- cording to available data and some simplified assumptions concerning the failure surface, the material strength and the physical mechanical properties. No numerical damping is employed. This is because although several damping models exist in the literature, few of them are underpinned by experimental evidence. Secondly, when modelling rockslides, and especially rapid ones, any damping would alter the mechanical behaviour exhibited by the system significantly.

Parameters	Value	Parameters	Value
DEM Parameters			
Number of grains, N	21,600–24,550	Shear stiffness, K_s (N/m)	2.7×10^9
Particle diameter, D (m)	[1.8, 3.8]	Rolling stiffness, K_r (N/m)	0
Density, ρ_s (kg/m^3)	2650	Inter-particle friction angle, θ (°)	30
Sample porosity, n	0.37–0.45	Basal friction angle, θ_b (°)	10
Normal stiffness, K_n (N/m)	3×10^9	Damping coefficient, β	0
CFD Parameters			
Water density, ρ_w (kg/m^3)	1000	Air density, ρ_a (kg/m^3)	1.225
Water viscosity, μ_w (Pa s)	0.001	Air viscosity, μ_a (Pa s)	1.8×10^{-5}
Simulation parameters			
Gravity, g (m/s^2)	9.81	CFD time step, Δt_2 (s)	1.0×10^{-3}
DEM time step, Δt_1 (s)	1.0×10^{-5}	Coupling frequency[a]	100

Table 1. Input parameters of the DEM-CFD model.

Figure 3 illustrates the evolution of slope deformation and the motion of water wave during the sliding of Vajont eastern slope (section A–A in Fig. 2b). The slope mass is initially coloured grey and green at different parallel layers, so that its deformation can be clearly identified during the rocksliding. It can be observed that at the beginning of the slide, the slope mass moves as a whole on the failure surface and quickly slides into the reservoir with a slight rotational component of motion, generating water waves. The water wave moves in the sliding direction and splashes onto the northern bank of the Vajont valley. Near the flow front, the CFD mesh cells are filled with both water and air, thus, the colour representing the water phase is less intense.

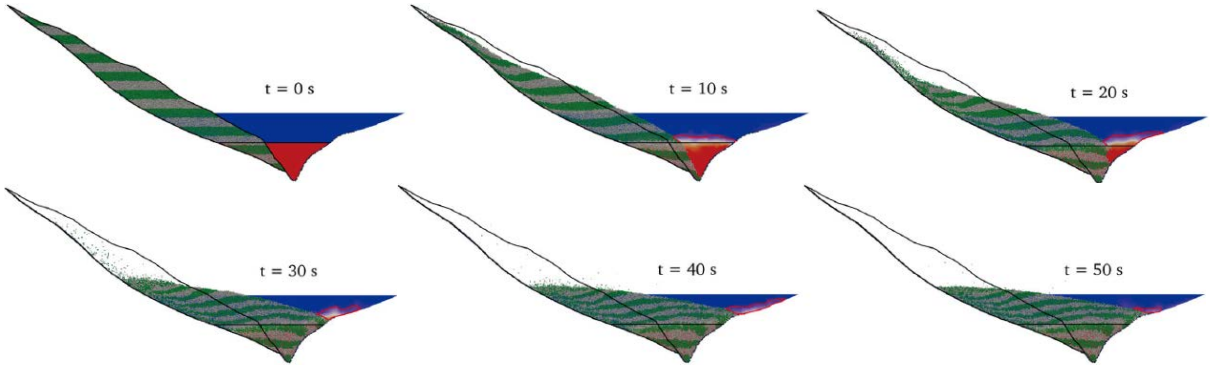

Fig. 3 Evolution of slope section A-A. The granular mass is initially coloured in horizontal stripes to follow the internal deformation. For the fluid domain, red and blue represent water and air respectively with the smear colour representing the air-water mixture. The splashed water wave is represented by regions enclosed by red curves.

The velocity of the water wave and its height time are illustrated in Figs. 4 and 5 respectively for the simulation of both sections considered, Easter and Western. It can be observed that the water waves move initially slowly towards as the slope mass slides into the reservoir. After 15 seconds and 8 seconds respectively from initiation, the wave velocities increase to their peaks value of 20 m/s and 18 m/s respectively. Then they decrease gradually to zero. After that (see the vertical dashed lines in the figures), the splashed water wave flows back into the reservoir, and above the slide mass as represented by the gradual increase of water wave velocity.

According to Fig. 10, it can be observed that the elevation of water wave increases gradually from zero to the peak value of 130 m. After reaching the maximum height at 43 s since the onset of the slope failure, it de- creases slowly due to the back flow of water into the reservoir. The final elevation of water in the reservoir is about 35 m above the initial reservoir water level.

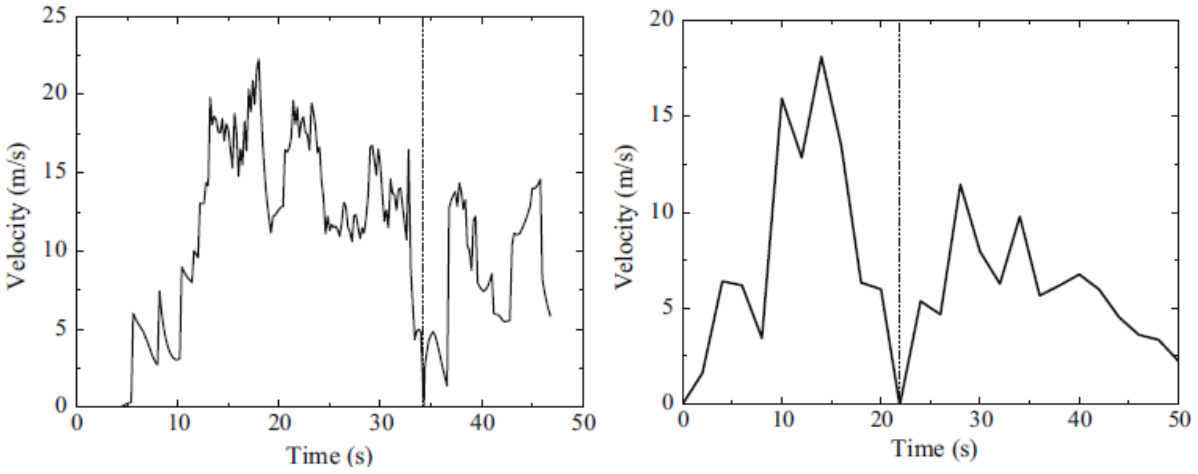

Fig. 4 Speed of the overtopping wave above the reservoir level: a) eastern section; b) western section.

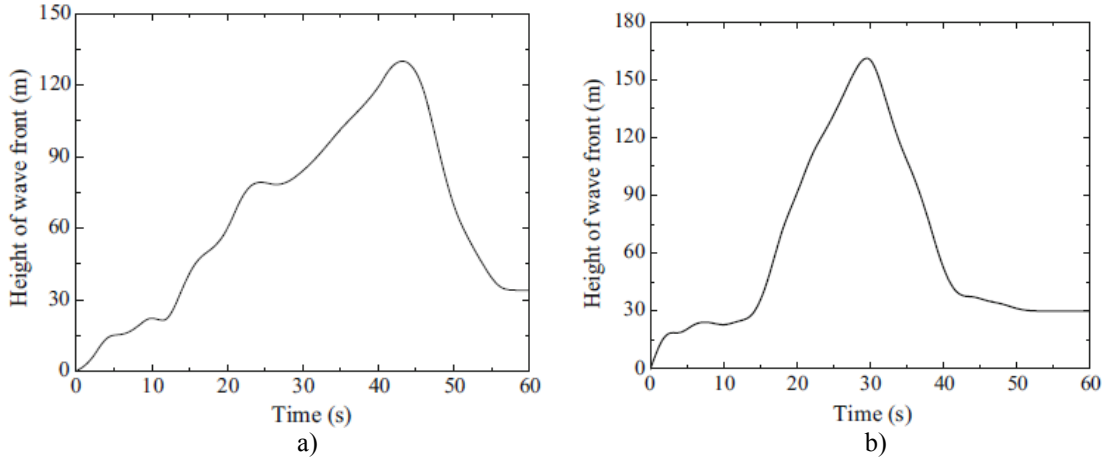

Fig. 5 Height of the overtopping wave above the reservoir level: a) eastern section; b) western section.

5 CONCLUSIONS

The current 3D plane strain DEM simulations have captured the general features (e.g. slope and wave motions) of the Vajont rockslide at the eastern and western sectors. The use of high fluid viscosity and coarse grain model has shown the possibility to model realistically both the slope and wave motions.

The average slope velocity for the slopes and the corresponding water wave velocities together with the maximum height of the wave runup on the opposite valley flank for both slopes turn out to be in very close to the field observations at the same spots.

ACKNOWLEDGMENTS

This project has received funding from the European Union's Horizon 2020 research and innovation programme under the Marie Skłodowska-Curie grant agreement No 645665.

REFERENCES

[1] Brideau, MA., Sturzenegger, M, Stead, D., Jaboyedoff, M., Lawrence, M., Roberts, NJ. and Clague JJ. (2012), Stability analysis of the 2007 Chehalis lake landslide based on long-range terrestrial photogrammetry and airborne LiDAR data, Landslides, 9(1), 75–91.

[2] Roberts, NJ., McKillop, RJ., Lawrence, MS., Psutka, JF., Clague, JJ., Brideau, MA. and Ward BC. (2013), Impacts of the 2007 landslide generated tsunami in Chehalis Lake, Canada, in Landslide Science and Practice, edited by C. Margottini , P. Canuti, and K. Sassa, pp. 133–140, Springer, Berlin.

[3] Miller, GS., Take, AW., Mulligan RP. and McDougall, S. (2017), Tsunamis generated by long and thin granular landslides in a large flume, J. Geophys. Res. Oceans, 122, doi:10.1002/2016JC012177.

[4] Mulligan, RP., Take, WA. (2017). On the transfer of momentum from a granular landslide to a water wave. Coastal Engineering, 125: 16-22.

[5] Semenza, E., Ghirotti, M. (2000) History of the 1963 Vaiont slide: the importance of geological factors. Bull Eng. Geol Env, 59: 87-97.

[6] Chowdhury, R. (1978) Analysis of the Vajont slide—new approach. Rock Mechanics 11(1): 29–38.

[7] Sakai, M., Takahashi, H., Pain, CC., Latham, J-P., Xiang, J. (2012) Study on a large-scale discrete element model for fine particles in a fluidized bed. Adv Powder Technol 23(5): 673–681

[8] Abe, S., Place, D., Mora, P. (2004) A parallel implementation of the lattice solid model for the simulation of rock mechanics and earthquake dynamics. Pure appl Geophys 161(11–12):2265–2277.

[9] OpenCFD (2004) OpenFOAM—The open source CFD toolbox, http://www.openfoam.com/

[10] Chen, F., Drumm, EC., Guiochon, G. (2011) Coupled discrete element and finite volume solution of two classical soil mechanics problems. Comput Geotech 38(5): 638–647.

[11] Zhao, T., Houlsby, GT., Utili, S. (2014). Investigation of granular batch sedimentation via DEM-CFD coupling. Granular matter, 16(6): 921-932.

[12] Jiang, MJ., Yu, HS., Harris, D. (2005) A novel discrete model for granular material incorporating rolling resistance. Comput Geotech 32(5): 340–357.

[13] Kafui, KD., Thornton, C., Adams, MJ. (2002) Discrete particle- continuum fluid modelling of gas–solid fluidised beds. Chem Eng Sci., 57(13):2395–2410

[14] Di Felice, R. (1994) The voidage function for fluid–particle interaction systems. Int J Mult. Flow 20(1): 153–159.

[15] Brown, P., Lawler, D. (2003) Sphere drag and settling velocity revisited. J Environ Eng 129(3): 222–231.

[16] Brennen, CE. (2005) Fundamentals of multiphase flow. Cambridge University Press, Cambridge.

[17] Hirt, CW., Nichols, BD. (1981) Volume of fluid (Vof) method for the dynamics of free boundaries. J Comput Phys, 39(1): 201–225.

[18] Zhao, T., Utili, S., Crosta, GB. (2016) Rockslide and impulse wave modelling in the Vajont reservoir by DEM-CFD analyses. Rock Mech Rock Eng 49: 2437-2456.